



The initial $^{41}\text{Ca}/^{40}\text{Ca}$ ratios in two type A Ca–Al-rich inclusions: Implications for the origin of short-lived ^{41}Ca

Ming-Chang Liu

Department of Earth, Planetary, and Space Sciences, UCLA, Los Angeles, CA, United States

Received 26 April 2016; accepted in revised form 16 October 2016; available online 26 October 2016

Abstract

This paper reports new ^{41}Ca – ^{41}K isotopic data for two Type A CAIs, NWA 3118 #1Nb (Compact Type A) and Vigarano 3138 F8 (Fluffy Type A), from reduced CV3 chondrites. The NWA CAI is found to have carried live ^{41}Ca at the level of $(4.6 \pm 1.9) \times 10^{-9}$, consistent with the proposed Solar System initial $^{41}\text{Ca}/^{40}\text{Ca} = 4.2 \times 10^{-9}$ by Liu et al. (2012a). On the other hand, the Vigarano CAI does not have resolvable radiogenic ^{41}K excesses that can be attributed to the decay of ^{41}Ca . Combined with the ^{26}Al data that have been reported for these two CAIs, we infer that the ^{41}Ca distribution was not homogeneous when ^{26}Al was widespread at the canonical level of $^{26}\text{Al}/^{27}\text{Al} = 5.2 \times 10^{-5}$. Such a ^{41}Ca heterogeneity can be understood under two astrophysical contexts: in situ charged particle irradiation by the protoSun in the solar nebula that had inherited some baseline ^{10}Be abundance from the molecular cloud, and Solar System formation in a molecular cloud enriched in ^{26}Al and ^{41}Ca contaminated by massive star winds. That said, more high quality ^{41}Ca data are still needed to better understand the origin of this radionuclide.

© 2016 Elsevier Ltd. All rights reserved.

Keywords: Meteorites, meteors, meteoroids; Secondary ion mass spectrometry; Short-lived radionuclides

1. INTRODUCTION

The origin of shortest-lived radionuclides ($t_{1/2} \leq 10$ Myr) provides important constraints on the birth environment of the Sun, and is also a crucial piece of information if one intends to use these radioactivities for early Solar System chronology. From theoretical viewpoints, these extinct radioisotopes could come into the forming Solar System as a stellar product, either from a dying star (supernova, asymptotic giant branch star, or Wolf–Rayet star; see e.g., Huss et al., 2009; Wasserburg et al., 2006; Arnould et al., 2006) or from the background molecular cloud Young (2014). Some radionuclides could also be a result of spallation-induced nuclear reactions between energetic charged particles (protons and alphas) and ambient gas/solid near the proto-Sun (e.g., Gounelle et al., 2006).

Radionuclides synthesized in the same process should in principle exhibit a concordant decay behavior.

The former existence of ^{41}Ca , which decays to ^{41}K with a half-life of 0.1 Myr, can be in theory accounted for by either stellar nucleosynthesis or in situ irradiation. If ^{41}Ca was derived from outside the solar nebula, not only would this radionuclide be potentially useful for chronology, but its initial abundance could set an upper limit for the timespan between the collapse of the parental molecular cloud and Solar System formation. On the contrary, spallation near the proto-Sun would have resulted in a ^{41}Ca heterogeneity in the solar nebula, rendering chronological interpretations difficult. However, it has not been possible to favor one source over the other because the limited amount of data available for ^{41}Ca has hindered our understanding of its initial abundance and distribution, and therefore its relationship with other short-lived radionuclides, in the early Solar System.

E-mail address: mcliu@ucla.edu

The prior presence of ^{41}Ca is inferred through the detection of radiogenic ^{41}K excesses ($\equiv^{41}\text{K}^*$) in the oldest dateable Solar System materials, namely Ca–Al-rich Inclusions (CAIs). However, such measurements require analytically challenging mass spectrometry (see below; also see Hutcheon et al., 1984; Srinivasan et al., 1996; Ito et al., 2006; Liu et al., 2012a for more details). Earlier work on the ^{41}Ca abundances in CAIs was performed on small-geometry secondary ion mass spectrometers (SIMS, such as CAMECA ims-3f and 4f), and these workers discovered large $^{41}\text{K}^*$ correlating with the $^{40}\text{Ca}/^{39}\text{K}$ ratios of the phases in CV3 (Allende and Efremovka) Type B CAIs (Hutcheon et al., 1984; Srinivasan et al., 1996; Sahijpal et al., 2000) and of CM2 (Murchison) hibonite grains ($\text{CaAl}_{12}\text{O}_{19}$) (Sahijpal and Goswami, 1998; Sahijpal et al., 2000). The results indicated that ^{41}Ca existed in the solar nebula with an initial abundance of $^{41}\text{Ca}/^{40}\text{Ca} \sim 1.4 \times 10^{-8}$. It was also found that short-lived ^{26}Al ($t_{1/2} = 0.7$ Myr) was correlated with ^{41}Ca in terms of presence or absence: when a CAI sample contains $^{41}\text{Ca}/^{40}\text{Ca} \sim 1.4 \times 10^{-8}$, it is normally characterized by $^{26}\text{Al}/^{27}\text{Al} = 5 \times 10^{-5}$. On the other hand, samples (e.g., CM2-chondrite platy hibonite crystals) lacking $^{41}\text{K}^*$ that could be due to the decay of ^{41}Ca are free of ^{26}Al (Sahijpal and Goswami, 1998; Sahijpal et al., 2000). Given that $^{26}\text{Al}/^{27}\text{Al} = 5.2 \times 10^{-5}$ having characterized the early solar nebula (or at least the CAI forming region) could have been a result of external seeding of ^{26}Al followed by hydrodynamic mixing (e.g. Boss, 2007, 2011), the correlation between ^{41}Ca and ^{26}Al implies that ^{41}Ca was also derived from an external source and was cogenetic with ^{26}Al (Sahijpal and Goswami, 1998).

Recent reanalysis with a large-geometry SIMS (CAMECA ims-1280HR2) of the CAI samples (Efremovka E44 and E65), in which $^{41}\text{Ca}/^{40}\text{Ca} = 1.4 \times 10^{-8}$ was primarily inferred (Srinivasan et al., 1996), revealed that their $^{41}\text{Ca}/^{40}\text{Ca}$ ratios were 7–10 times lower than the previously determined value (Liu et al., 2012a). After correcting for the resetting time calculated from the sub-canonical $^{26}\text{Al}/^{27}\text{Al}$ ratios reported for these two inclusions (Young et al., 2005; Srinivasan and Chaussidon, 2013), Liu et al. (2012a) found a converging $^{41}\text{Ca}/^{40}\text{Ca}$ ratio $\sim 4 \times 10^{-9}$, perfectly consistent with the $^{41}\text{Ca}/^{40}\text{Ca}$ value by Ito et al. (2006) in the Allende EGG3 CAI that is also characterized by canonical $^{26}\text{Al}/^{27}\text{Al} = (5.29 \pm 0.39) \times 10^{-5}$ (Wasserburg et al., 2012). Based on this apparent synchronicity between the two radionuclides, Liu et al. (2012a) proposed that $^{41}\text{Ca}/^{40}\text{Ca} \sim 4 \times 10^{-9}$ should be the best representative initial abundance in the early Solar System and that ^{26}Al and ^{41}Ca should have come into the Solar System together as stellar products.

It should be pointed out that the synchronicity between ^{26}Al and ^{41}Ca was inferred based on the data reported for three CAIs, which are all Type B inclusions. Petrological examinations showed that Type Bs have complicated thermal histories, e.g., multiple-stage (partial) remelting and (partial) recrystallization. Sometimes such processing could make the ^{26}Al data difficult to decipher (e.g. MacPherson et al., 2012). Therefore, Type Bs are not good targets for

constraining the Solar System $^{41}\text{Ca}/^{40}\text{Ca}$ initial value. Instead, samples that appear to have escaped remelting since their formation, such as Fluffy Type A (FTA) CAIs, should be used. In hopes of further testing the concordant decay behavior of ^{26}Al and ^{41}Ca , samples that have sub-canonical $^{26}\text{Al}/^{27}\text{Al}$ ratios corresponding to $\sim (1-2) \times 10^5$ years compared to 5.2×10^{-5} would be needed. In this paper, we report the ^{41}Ca – ^{41}K isotopic results of two Type A CAIs from reduced CV3 chondrites, NWA 3118 and Vigarano, and discuss possible origins of short-lived ^{41}Ca .

2. EXPERIMENTAL

2.1. Samples

The samples used in this study are the NWA 3118 #1Nb (Compact Type A, “CTA”) and Vigarano 3138 F8 (FTA) CAIs. The NWA 3118 and Vigarano chondrites are reduced CV3; therefore, CAIs within them should have experienced less secondary processing than those in oxidized CV3 chondrites, such as Allende. Detailed petrological and mineralogical descriptions of the two CAIs can be found in MacPherson et al. (2012, 2013). In general, the samples are petrologically free of secondary alteration and coarse-grained, making them suitable for the K isotope measurements. Recent high precision Mg isotope analyses of the two CAIs revealed well-defined ^{26}Al isochrons with very little scatter, with NWA 3118 #1Nb and Vigarano 3138 F8 being characterized by $^{26}\text{Al}/^{27}\text{Al} = (4.64 \pm 0.09) \times 10^{-5}$ ($\chi^2 = 1.5$) and $^{26}\text{Al}/^{27}\text{Al} = (5.29 \pm 0.28) \times 10^{-5}$ ($\chi^2 = 1.9$), respectively (MacPherson et al., 2012; MacPherson et al., 2013). The canonical $^{26}\text{Al}/^{27}\text{Al}$ ratio, along with the petrological texture of Vigarano 3138 F8, suggests that this CAI has never experienced post-formation remelting and isotopic resetting (at least for Mg). The very tight isochron derived for the CTA indicates that no isotopic disturbance took place after the last melting event. The difference in the $^{26}\text{Al}/^{27}\text{Al}$ ratio between FTA and CTA can be translated to a $\sim 100,000$ year timespan, which is the half-life of ^{41}Ca . Therefore, if the synchronicity between ^{26}Al and ^{41}Ca holds, one should expect that Vigarano 3138 F8 contains twice as much $^{41}\text{Ca}/^{40}\text{Ca}$ as does NWA 3118 #1Nb.

2.2. Ion microprobe techniques

Measurements of K isotopes were carried out on the new CAMECA 1290 ion microprobe at UCLA by following the analytical protocol developed by Liu et al. (2012a). A polished sample was sputtered with a 10 nA, 23 keV $^{16}\text{O}^-$ primary beam ($\phi \sim 20 \mu\text{m}$). 25 min presputtering was applied to the sample prior to each spot analysis to minimize the surface contaminations. The field aperture with a width of 2500 μm was used to block out scattered K ions from the edge of the analysis crater. The mass resolution ($M/\Delta M$) was set at 8000, which is sufficient to fully separate $^{41}\text{K}^+$ from $^{40}\text{CaH}^+$ and other minor interferences from the peaks of interest, but is incapable of resolving $(^{40}\text{Ca}^{42}\text{Ca})^{++}$ from $^{41}\text{K}^+$ ($M/\Delta M = 34,000$ is required). Therefore, the contribution of $(^{40}\text{Ca}^{42}\text{Ca})^{++}$ at $m/e = 41$

was estimated indirectly by using the following equality (Hutcheon et al., 1984; Srinivasan et al., 1996):

$$\frac{({}^{40}\text{Ca}^{42}\text{Ca})^{++}}{{}^{42}\text{Ca}^+} = \frac{({}^{40}\text{Ca}^{43}\text{Ca})^{++}}{{}^{43}\text{Ca}^+}$$

The measured $({}^{40}\text{Ca}^{43}\text{Ca})^{++}/{}^{43}\text{Ca}^+$ ratio in each spot analysis was used to estimate $({}^{40}\text{Ca}^{42}\text{Ca})^{++}$. It should be noted that the fraction of this component comprising the total signal at $m/e = 41$ is proportional to ${}^{40}\text{Ca}/{}^{39}\text{K}$. Liu et al. (2012a) showed that more than 85% of counts at mass 41 come from ${}^{40}\text{Ca}^{42}\text{Ca}^{++}$ in phases with ${}^{40}\text{Ca}/{}^{39}\text{K} \geq 10^7$, whereas this percentage drops down to $\sim 20\%$ when ${}^{40}\text{Ca}/{}^{39}\text{K} \sim 10^6$. The correction for $({}^{40}\text{Ca}^{43}\text{Ca})^{++}$ becomes essentially insignificant for phases that have ${}^{40}\text{Ca}/{}^{39}\text{K} \leq 10^5$.

Besides $({}^{40}\text{Ca}^{42}\text{Ca})^{++}$, we also carefully quantified the levels of scattered ions from the tails of ${}^{40}\text{Ca}^+$ and ${}^{40}\text{CaH}^+$ at $m/e = 41$. The former and the latter were found to be $\sim 1.4 \times 10^{-10} \times {}^{40}\text{Ca}^+$ and $1.8 \times 10^{-5} \times {}^{40}\text{CaH}^+$, respectively. Although insignificant compared to $({}^{40}\text{Ca}^{42}\text{Ca})^{++}$, the tailing effects were still corrected for. The dynamic background of the counting system was measured for 60 s at mass 38.7 at the beginning of each analytical cycle, and the count rate falls within 0.02 to 0.05 counts per second, similar to what was found on the CAMECA 1280HR2 by Liu et al. (2012a). This background was used instead of the static background of ~ 0.003 counts per second measured without the ion beam on overnight for 10 h. The true ${}^{41}\text{K}/{}^{39}\text{K}$ ratio of a spot was obtained after summing up counts over the entire analytical cycles (Ogliore et al., 2011) and stripping off the interferences:

$$\left(\frac{{}^{41}\text{K}^+}{{}^{39}\text{K}^+}\right)_{\text{true}} = \frac{[41]_{\text{m}} - \left[\frac{({}^{40}\text{Ca}^{43}\text{Ca})^{++}}{{}^{43}\text{Ca}^+}\right] \times {}^{42}\text{Ca}^+ - [{}^{40}\text{CaH}^+]_{\text{tail}} - [{}^{40}\text{Ca}^+]_{\text{tail}} - \text{bkgd}}{{}^{39}\text{K}^+}$$

The delta-notation is expressed as:

$$\delta^{41}\text{K}(\text{‰}) = \left(\frac{\left(\frac{{}^{41}\text{K}^+}{{}^{39}\text{K}^+}\right)_{\text{true}}}{0.072} - 1 \right) \times 1000$$

where 0.072 is terrestrial ${}^{41}\text{K}/{}^{39}\text{K}$ (Garner et al., 1975).

Secondary ions, with a mass sequence of 38.7, ${}^{39}\text{K}^+$, ${}^{41}\text{K}^+$, ${}^{40}\text{CaH}^+$, $({}^{40}\text{Ca}^{43}\text{Ca})^{++}$, $({}^{40}\text{Ca}^{27}\text{Al}^{16}\text{O})^{++}$, ${}^{42}\text{Ca}^+$ and ${}^{43}\text{Ca}^+$, were collected with the axial electron multiplier (EM) in peak-switching mode. The ${}^{41}\text{K}^+$ and $({}^{40}\text{Ca}^{42}\text{Ca})^{++}$ peaks were counted for 60 s to achieve sufficient counting statistics. Each spot analysis was composed of 25–50 cycles, depending on the ${}^{41}\text{K}^+$ count rate, and could take up to 4 h. To compensate for drifts in magnetic field and surface charging during a long analysis, both mass calibration and energy centering were performed automatically every five cycles. A terrestrial calcite standard with ${}^{40}\text{Ca}/{}^{39}\text{K} > 10^6$ and a diopside standard (${}^{40}\text{Ca}/{}^{39}\text{K} > 10^5$) (see Fig. 1) were used to ascertain that corrections for interferences at $m/e = 41$ were properly carried out. It can be seen that the instrumental mass fractionation and matrix effect on K isotope compositions were negligible compared to counting errors, and therefore would not affect the determination of ${}^{41}\text{K}$ excesses in CAIs.

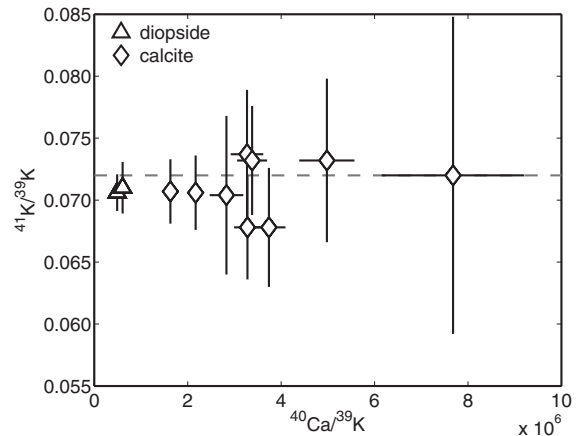


Fig. 1. The potassium isotopic compositions of two standard minerals. That all standard points have terrestrial ${}^{41}\text{K}/{}^{39}\text{K} = 0.072$ (gray dashed line) over a large range of ${}^{40}\text{Ca}/{}^{39}\text{K}$ (up to $\sim 8 \times 10^6$) suggests appropriate corrections for $({}^{40}\text{Ca}^{42}\text{Ca})^{++}$.

The relative sensitivity factor (RSF) of Ca to K was determined to be 2.20 ± 0.02 (2σ) on a piece of NIST 616 glass ($\text{CaO} = 12\%$ and $\text{K} = 29 \mu\text{g g}^{-1}$). The true ${}^{40}\text{Ca}/{}^{39}\text{K}$ ratio of a measured spot is calculated as follows:

$$\left(\frac{{}^{40}\text{Ca}}{{}^{39}\text{K}}\right)_{\text{true}} = \left(\frac{{}^{42}\text{Ca}^+}{{}^{39}\text{K}^+}\right)_{\text{m}} \times \frac{{}^{40}\text{Ca}}{{}^{42}\text{Ca}} \times \text{RSF},$$

where ${}^{40}\text{Ca}/{}^{42}\text{Ca} = 151.03$ (Niederer and Papanastassiou, 1984).

3. RESULTS

The potassium isotopic compositions of NWA 3118 #1Nb and Vigarano 3138 F8 are tabulated in Table 1 and plotted in Fig. 2. In the NWA CAI, all the analyses were performed on fassaite crystals. Compared to the E44 and E65 samples measured by Liu et al. (2012a) where very high ${}^{40}\text{Ca}/{}^{39}\text{K}$ ratios (up to 10^7) were found, this sample appears to be more contaminated with potassium, and the highest ${}^{40}\text{Ca}/{}^{39}\text{K}$ ratios are around $\sim 1 \times 10^6$. The data show a correlation between ${}^{41}\text{K}^*$ and ${}^{40}\text{Ca}/{}^{39}\text{K}$, and the slope of an error-weighted fit yields a ${}^{41}\text{Ca}/{}^{40}\text{Ca}$ ratio of $(4.7 \pm 1.9) \times 10^{-9}$ (2σ), with a $\tilde{\chi}^2$ value of 14.2 (Fig. 2a, upper panel). If the gray-filled data point (NWA-fas4) is excluded from the regression due to its anomalously low (subchondritic) ${}^{41}\text{K}/{}^{39}\text{K}$ (0.0701), a very similar ${}^{41}\text{Ca}/{}^{40}\text{Ca}$ ratio of $(4.6 \pm 1.9) \times 10^{-9}$ with improved (albeit imperfect) $\tilde{\chi}^2 = 7.4$ is derived. This seemingly large $\tilde{\chi}^2$ value results from the fact that the four data points with low ${}^{40}\text{Ca}/{}^{39}\text{K}$ ratios (NWA-fas2, NWA-fas3, NWA-fas5 and NWA-fas7) are deviated from the best-fit line by $2.5\text{--}4\sigma$. This could be due to somewhat underestimated analytical errors, which are calculated by using Poisson statistics with total counts, rather than using the ratio variations on a cycle-by-cycle basis. This is because under our analytical condition, the typical intensity of $({}^{40}\text{Ca}^{43}\text{Ca})^{++}$, the peak used to quantify the contribution of $({}^{40}\text{Ca}^{42}\text{Ca})^{++}$ at mass 41 (see above), in fassaite is ~ 2 counts s^{-1} . To avoid statistical

Table 1
Potassium isotopic compositions of NWA 3118 #1Nb and Vigarano 3138 F8 CAIs

Sample	$^{40}\text{Ca}/^{39}\text{K}$ ($\pm 2\sigma$)	$^{41}\text{K}/^{39}\text{K}$ ($\pm 2\sigma$)*	$\delta^{41}\text{K}$ ($\pm 2\sigma$)
NWA-fas1	$(1.02 \pm 0.06) \times 10^6$	0.07421 ± 0.00531	$30.65 \pm 73.77\%$
NWA-fas2	$(1.50 \pm 0.01) \times 10^4$	0.07233 ± 0.00022	$4.58 \pm 3.03\%$
NWA-fas3	$(6.57 \pm 0.03) \times 10^3$	0.07139 ± 0.00014	$-8.53 \pm 2.01\%$
NWA-fas4	$(2.57 \pm 0.02) \times 10^4$	0.07011 ± 0.00034	$-26.28 \pm 4.74\%$
NWA-fas5	$(3.86 \pm 0.02) \times 10^4$	0.07243 ± 0.00024	$5.99 \pm 3.36\%$
NWA-fas6	$(1.16 \pm 0.03) \times 10^5$	0.07210 ± 0.00109	$1.45 \pm 15.13\%$
NWA-fas7	$(6.44 \pm 0.08) \times 10^4$	0.07265 ± 0.00050	$9.07 \pm 7.01\%$
NWA-fas8	$(7.78 \pm 0.13) \times 10^4$	0.07186 ± 0.00069	$-1.91 \pm 9.57\%$
NWA-fas9	$(1.22 \pm 0.06) \times 10^6$	0.07729 ± 0.00480	$73.50 \pm 66.69\%$
NWA-fas10	$(1.08 \pm 0.02) \times 10^5$	0.07197 ± 0.00079	$-0.38 \pm 10.97\%$
NWA-fas11	$(1.03 \pm 0.01) \times 10^5$	0.07160 ± 0.00057	$-5.49 \pm 7.96\%$
NWA-fas12	$(3.09 \pm 0.13) \times 10^5$	0.07106 ± 0.00241	$-13.08 \pm 33.42\%$
NWA-fas13	$(1.66 \pm 0.04) \times 10^5$	0.07222 ± 0.00111	$3.00 \pm 15.39\%$
NWA-fas14	$(2.58 \pm 0.08) \times 10^5$	0.07150 ± 0.00162	$-6.93 \pm 22.52\%$
NWA-fas15	$(3.84 \pm 0.10) \times 10^5$	0.07428 ± 0.00160	$31.62 \pm 22.17\%$
Vig-mel1	$(9.29 \pm 0.23) \times 10^4$	0.07150 ± 0.00100	$-6.90 \pm 13.84\%$
Vig-mel2	$(4.37 \pm 0.09) \times 10^5$	0.07175 ± 0.00110	$-3.50 \pm 15.24\%$
Vig-mel3	$(6.35 \pm 0.06) \times 10^4$	0.07214 ± 0.00040	$1.98 \pm 5.53\%$
Vig-mel4	$(1.37 \pm 0.04) \times 10^5$	0.07242 ± 0.00124	$5.81 \pm 17.28\%$
Vig-mel5	$(4.03 \pm 0.05) \times 10^4$	0.07287 ± 0.00050	$12.12 \pm 6.93\%$
Vig-mel6	$(4.18 \pm 0.16) \times 10^5$	0.07242 ± 0.00194	$5.88 \pm 27.00\%$
Vig-mel7	$(7.99 \pm 0.10) \times 10^4$	0.07114 ± 0.00051	$-11.96 \pm 7.15\%$
Vig-mel8	$(9.11 \pm 0.13) \times 10^4$	0.07226 ± 0.00056	$3.58 \pm 7.74\%$
Vig-mel9	$(2.66 \pm 0.08) \times 10^5$	0.07062 ± 0.00134	$-19.21 \pm 18.57\%$
Vig-fas1	$(8.94 \pm 0.09) \times 10^4$	0.07179 ± 0.00042	$-2.91 \pm 5.79\%$
Vig-fas2	$(1.90 \pm 0.02) \times 10^4$	0.06948 ± 0.00030	$-35.05 \pm 4.20\%$

* The error of true $^{41}\text{K}/^{39}\text{K}$ was calculated by propagating the counting errors of stripped components ($(^{40}\text{Ca}^{42}\text{Ca})^{++}$, $^{40}\text{CaH}_{\text{tail}}^+$ and $^{40}\text{Ca}_{\text{tail}}^+$) into those of potassium isotopes. From counting statistics, $(^{40}\text{Ca}^{42}\text{Ca})^{++}$ contributes roughly $<2\%$ to the final error of $^{41}\text{K}/^{39}\text{K}$, whereas the contributions from $^{40}\text{CaH}_{\text{tail}}^+$ and $^{40}\text{Ca}_{\text{tail}}^+$ are negligible because the two components comprise $<1\%$ of the total signals at mass 41.

ratio bias that may occur under such low count rates (Ogliore et al., 2011; Coath et al., 2013), and thus to accurately determine $^{41}\text{K}/^{39}\text{K}$, summing up all the counts before stripping off $(^{40}\text{Ca}^{42}\text{Ca})^{++}$ (see above for the equation for obtaining $^{41}\text{K}/^{39}\text{K}$) is necessary. Estimations of errors based on cycle-by-cycle ratio variations would be in conflict with the way that the $^{41}\text{K}/^{39}\text{K}$ ratios were calculated. Although the analytical uncertainties for NWA-fas2, NWA-fas3, NWA-fas5 and NWA-fas7 could be somewhat underestimated, these points do not affect the slope of the best-fit line. Therefore, we argue that a $\tilde{\chi}^2$ value of 7.4 does not render this correlation line invalid, and that $^{41}\text{Ca}/^{40}\text{Ca} = (4.6 \pm 1.9) \times 10^{-9}$ represents the initial value for this CAI.

In the Vigarano 3138 F8 CAI, the majority of analysis spots were made on melilite crystals (Fig. 2b, lower panel). Fassaite is less abundant compared to melilite, and has been studied previously for ^{26}Al - ^{26}Mg (MacPherson et al., 2012). Therefore, only two spot measurements were performed on fassaite. This sample contains more potassium than NWA 3118 #1Nb; all spots have $^{40}\text{Ca}/^{39}\text{K}$ less than 10^6 . Error-weighted regression through all the data points gives rise to a $^{41}\text{Ca}/^{40}\text{Ca}$ ratio of $(5.6 \pm 2.2) \times 10^{-9}$ (2σ), similar to that inferred for the NWA CAI within errors, but the goodness of fit is poor ($\tilde{\chi}^2 = 22.5$). It is because of the low $^{41}\text{K}/^{39}\text{K}$ ratio obtained from one fassaite spot (gray-filled point, Vig-fas2). The exclusion of this

anomalous spot from the regression not only yields a much smaller $\tilde{\chi}^2$ value (from 22.5 to 3.6), but also changes the inferred $^{41}\text{Ca}/^{40}\text{Ca}$ ratio to $(-2.0 \pm 2.5) \times 10^{-9}$, which suggests essentially no resolvable $^{41}\text{K}^*$. Given the better goodness of fit, $^{41}\text{Ca}/^{40}\text{Ca} = (-2.0 \pm 2.5) \times 10^{-9}$ is accepted as the initial abundance for Vigarano 3138 F8.

One observation that requires further investigations is subchondritic $^{41}\text{K}/^{39}\text{K}$ ($\delta^{41}\text{K} \sim -30 \pm 5\%$, see NWA-fas15 and Vig-fas2 in Table 1) characterizing a fassaite crystal in each CAI. Such low $\delta^{41}\text{K}$ values cannot have been a consequence of overcorrection for $(^{40}\text{Ca}^{42}\text{Ca})^{++}$ because these spots have $^{40}\text{Ca}/^{39}\text{K}$ ratios only $\sim 20,000$. Kinetic condensation during the formation of CAI precursors could have accounted for subchondritic $^{41}\text{K}/^{39}\text{K}$. It is possible that such condensation-derived K isotopic signatures were overprinted by mass-dependent fractionation associated with subsequent thermal processing, so that very little trace of this condensation record was kept in the CAIs. The existence of one subchondritic $^{41}\text{K}/^{39}\text{K}$ spot in the NWA CAI can be qualitatively understood in this context, as the petrological texture of this inclusion is indicative of partial melting (MacPherson et al., 2013). However, it would be difficult to explain the observation in the Vigarano CAI with this scenario. Because this inclusion is possibly of condensation origin and has remained unmelted since its formation (MacPherson et al., 2012), one would expect that $^{41}\text{K}/^{39}\text{K}$ reflecting a condensation process should be more

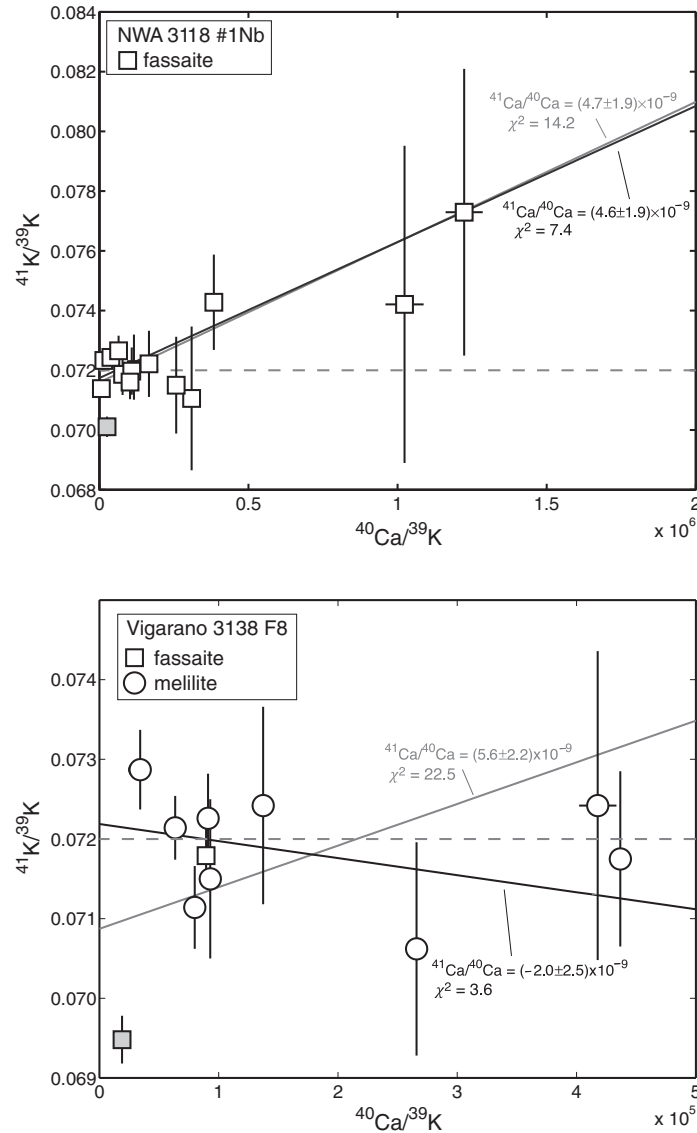


Fig. 2. The potassium isotopic compositions of NWA 3118 #1Nb (upper panel) and Vigarano 3138 F8 (lower panel) CAIs. The solid gray line in each panel is the best fit to all the data points, and the black line is the best fit without including the gray-filled point in the regression (see text). Dashed lines represent the terrestrial $^{41}\text{K}/^{39}\text{K}$ value of 0.072. All errors are 2σ .

widespread, as opposed to being seen in one out of 11 spots. Clearly more work needs to be conducted to have a better understanding of the meaning of these low $^{41}\text{K}/^{39}\text{K}$ ratios.

4. DISCUSSION

The data obtained in this study represent the first estimates of ^{41}Ca abundances in Type A CAIs from reduced CV3 chondrites. NWA 3118 #1Nb is a CTA CAI. The petrological textures and Mg isotope data ($^{26}\text{Al}/^{27}\text{Al} = (4.64 \pm 0.09) \times 10^{-5}$) both indicate that this sample has been thermally processed to a certain degree (e.g., partial melting, MacPherson et al., 2013) after its formation. However, the inferred $^{41}\text{Ca}/^{40}\text{Ca} = (4.6 \pm 1.9) \times 10^{-9}$ in this CAI is consistent with the Solar System initial value proposed by Liu et al. (2012a). In contrast, the Vigarano

3138 F8 CAI, which belongs to the FTA group, appears to have remained intact petrologically and isotopically (at least for Mg, $^{26}\text{Al}/^{27}\text{Al} = (5.29 \pm 0.28) \times 10^{-5}$) since it formed, but shows no resolvable $^{41}\text{K}^*$ that could be attributed to the decay of ^{41}Ca ($^{41}\text{Ca}/^{40}\text{Ca} = (-2.1 \pm 2.5) \times 10^{-9}$). Clearly, the ^{41}Ca abundances in the two CAIs with different thermal histories are not consistent with the concordant decay between ^{26}Al and ^{41}Ca , contrasting with the previous results found by Sahijpal and Goswami (1998), Sahijpal et al. (2000) and Liu et al. (2012). It should be pointed out that the lack of correlation between the two radionuclides has been previously reported for one CTA CAI (7R-19-1) from the Allende meteorite by Ito et al. (2006). Table 2 and Fig. 3 show a list of CAIs in which both ^{26}Al and ^{41}Ca abundances have been inferred by using large-radius ion microprobes (except for E44, whose Mg

Table 2

CAI samples of various Types and their inferred ^{26}Al and ^{41}Ca abundances measured by using large-radius ion microprobes

CAI	Type	$^{26}\text{Al}/^{27}\text{Al}$	$^{41}\text{Ca}/^{40}\text{Ca}$	$^{41}\text{Ca}/^{40}\text{Ca}_i^a$	Data source ^b
E44	Type B	$(4.8 \pm 0.3) \times 10^{-5}$	$(2.6 \pm 0.9) \times 10^{-9}$	4.55×10^{-9}	1,2
E65	Type B	$(4.46 \pm 0.25) \times 10^{-5}$	$(1.4 \pm 0.6) \times 10^{-9}$	4.1×10^{-9}	3,2
EGG3	Type B	$(5.23 \pm 0.13) \times 10^{-5}$	$(4.1 \pm 2.0) \times 10^{-9}$	4.1×10^{-9}	4,5
7R-19-1	CTA	$(6.6 \pm 1.3) \times 10^{-5}$	Not Detected	–	5
3138 F8	FTA	$(5.29 \pm 0.28) \times 10^{-5}$	Not Detected	–	6, this study
3118 #1Nb	CTA	$(4.64 \pm 0.09) \times 10^{-5}$	$(4.6 \pm 1.9) \times 10^{-9}$	1×10^{-8}	7, this study

^a The “initial” $^{41}\text{Ca}/^{40}\text{Ca}$ ratio after scaling $^{26}\text{Al}/^{27}\text{Al}$ back to 5.2×10^{-5} .

^b Data source: 1. Young et al. (2005); 2. Liu et al. (2012a); 3. Srinivasan and Chaussidon (2013); Wasserburg et al. (2012); 5. Ito et al. (2006); MacPherson et al. (2012); 7. MacPherson et al. (2013)

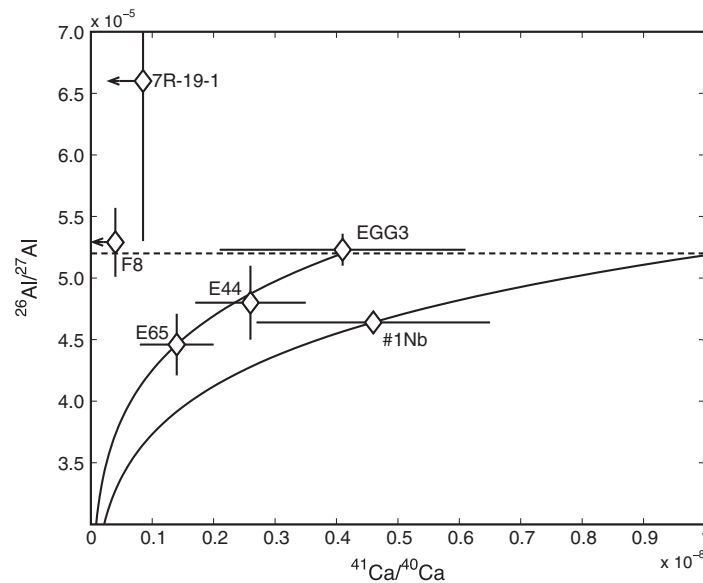


Fig. 3. $^{26}\text{Al}/^{27}\text{Al}$ vs. $^{41}\text{Ca}/^{40}\text{Ca}$ for 6 CAIs listed in Table 2. The two solid curves show how the two radionuclides would have decayed together. This plot shows that when $^{26}\text{Al}/^{27}\text{Al} = 5.2 \times 10^{-5}$ (dashed line), there could have been three reservoirs/populations of ^{41}Ca .

isotopes were measured by Laser Ablation Inductively Coupled Plasma Mass Spectrometry by Young et al. (2005)). In the following sections, we first argue for the legitimacy of the isochron derived for the NWA CAI, and then discuss the implications of these data for the initial abundance and distribution of ^{41}Ca in the Solar System and for the astrophysical origin of this radioactivity.

4.1. Is the correlation line in NWA 3118 #1Nb a valid isochron?

The NWA 3118 #1Nb CAI is characterized by relative low $^{40}\text{Ca}/^{39}\text{K}$ compared to, for example, E44 and E65 (e.g., Srinivasan et al., 1996; Liu et al., 2012a) CAIs. One potential concern derived from such low $^{40}\text{Ca}/^{39}\text{K}$ ratios is that the magnitude of ^{41}K excesses could also be understood as a result of isotopic fractionation associated with evaporation. Experimental studies have shown that Rayleigh fractionation could yield $\delta^{41}\text{K}$ up to 63‰ in an evaporation residue of initially chondritic composition when ~95% of K is lost (Richter et al., 2011). Indeed all the observed $\delta^{41}\text{K}$ values (see Table 1) in this CAI essentially

fall into this range within errors, but the distribution of the data points on an isochron plot cannot be explained by using a Rayleigh-type process. To demonstrate this, a Rayleigh fractionation curve as a function of $^{40}\text{Ca}/^{39}\text{K}$ is constructed by following the equation:

$$\left(\frac{^{41}\text{K}}{^{39}\text{K}}\right)_r = \left(\frac{^{41}\text{K}}{^{39}\text{K}}\right)_{\text{ini}} \times f^{(\alpha-1)}$$

$(^{41}\text{K}/^{39}\text{K})_r$ is the ratio in the evaporation residue, and $(^{41}\text{K}/^{39}\text{K})_{\text{ini}}$ is the initial ratio, which is assumed to be terrestrial (= 0.072). “ f ” is the fraction of potassium remaining in the residue; an initial bulk [K] = 30 ppm, which is roughly an average bulk potassium content reported for CTA CAIs by Sylvester et al. (1993), is assumed for the CAI. α is the kinetic isotope fractionation factor, and a value of 0.9790, derived by Richter et al. (2011) from their evaporation experiment, is adopted in the calculation. The calculation result is plotted alongside the data points in Fig. 4. As can be seen, the data points do not distribute along the Rayleigh fractionation curve, and evaporation-induced fractionation would have had a larger effect on $^{41}\text{K}/^{39}\text{K}$ than does the decay of ^{41}Ca within the range of

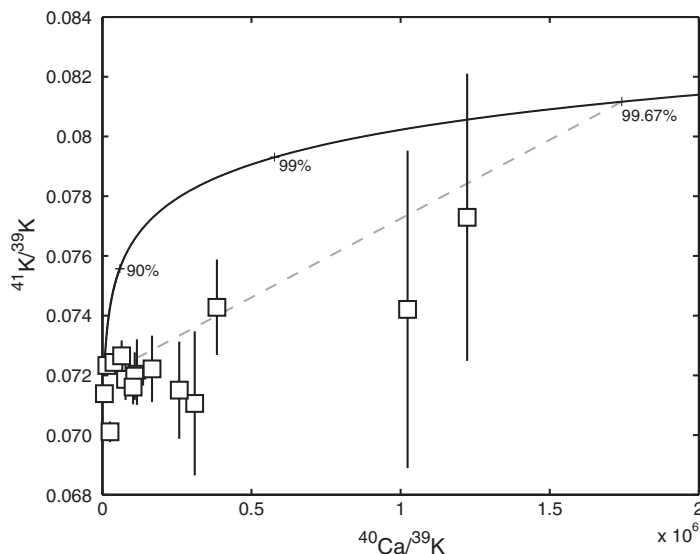


Fig. 4. The solid curve represents the expected $^{41}\text{K}/^{39}\text{K}$ variation as a result of Rayleigh fractionation. Plus signs indicate the amount of evaporative loss of K. Mixing between a residue that has lost ~ 99.6 – 99.8% of its initial K and a chondritic component results in a line with the slope consistent with the inferred $^{41}\text{Ca}/^{40}\text{Ca} = 4.6 \times 10^{-9}$. See text for more details.

$^{40}\text{Ca}/^{39}\text{K}$ ratios obtained in the NWA 3118 #1Nb CAI. This indicates that the observed correlation between ^{41}K excesses and $^{40}\text{Ca}/^{39}\text{K}$ could not have been a consequence of a Rayleigh-type process.

A mechanism that could potentially result in a correlation between $^{41}\text{K}/^{39}\text{K}$ and $^{40}\text{Ca}/^{39}\text{K}$ in a CAI involves evaporative loss of K followed by post-recrystallization mixing with normal K. It can be seen in Fig. 4 that the data can be well explained if a residue which has lost ~ 99.6 – 99.8% of initial K mixes with a chondritic reservoir ($^{41}\text{K}/^{40}\text{K} = 0.072$). This mixing line would have a slope $\sim 5 \times 10^{-9}$, comparable to the proposed $^{41}\text{Ca}/^{40}\text{Ca}$ ratio for NWA 3118 #1Nb. It is almost certain that the NWA CAI had lost a significant amount of initial K due to evaporation given that it has undergone partial melting (MacPherson et al., 2013). In addition, the Mg mass-dependent isotopic fractionation that characterizes essentially all compact Type A CAIs (on the order of a few ‰/amu, e.g., Jacobsen, 2008; MacPherson et al., 2012) requires that ~ 10 – 50% of the CAI's initial Mg content be lost during evaporation (Richter et al., 2007). When such extensive Mg loss occurred, it is likely that $>99\%$ of initial K would have already been driven out of the (partially) molten CAI (the experiment of Richter et al. (2011) showed that the Mg content remained unchanged when a chondritic melt has lost $\sim 95\%$ of initial K at 1470°C). A later addition of isotopically normal K could have taken place by diffusion after recrystallization of the CAI, leading to a mixing line similar to that shown in Fig. 4. However, we argue that the Mg isotopes of CAI constituents would be compromised if there was diffusive mixing. This is because the diffusivities of K and Mg in fassaite are essentially identical (e.g., 1.5×10^{-19} and $1.2 \times 10^{-19} \text{ m}^2 \text{ s}^{-1}$, respectively, at 1200°C ; approximated by using diopside; Ito et al., 2003; Zhang et al., 2008). In melilite, K diffuses even slower than does Mg (e.g., 5.5×10^{-19} and $9.4 \times 10^{-19} \text{ m}^2 \text{ s}^{-1}$ at

1200°C , respectively; Ito et al., 2006). The ^{41}Ca – ^{41}K correlation line observed in the NWA CAI is derived from the measurements of fassaite, and these fassaite crystals fall on a sub-canonical ^{26}Al – ^{26}Mg isochron ($^{26}\text{Al}/^{27}\text{Al} = 4.64 \times 10^{-5}$, $\chi^2 = 1.5$) alongside melilite and spinel with very little scatter (MacPherson et al., 2013). The Mg isotope result indicates that the CAI constituents remained undisturbed after the last melting event. Therefore, similar intactness for K isotopes in fassaite should be expected.

Given that Rayleigh-type fractionation or mixing between an evaporation residue and a chondritic reservoir cannot have led to the observed correlation between ^{41}K excesses and $^{40}\text{Ca}/^{39}\text{K}$, we are left with the possibility that the line represents an isochron from the decay of ^{41}Ca . One thing worth noting is that the intrinsic mass-dependent isotope fractionation effects usually need to be corrected for when deriving the radiogenic component, an exercise that is performed every time for Mg isotopes (e.g., Ireland et al., 1992; Liu et al., 2009; MacPherson et al., 2012). Theoretical predictions and laboratory experiments both show that the larger the depletion in an elemental abundance in a residue, the more mass-dependently fractionated the isotopic composition of that element (e.g., Richter et al., 2007). It is true that the intrinsic K mass-dependent fractionations were not corrected for due to the fact that $^{40}\text{K}^+$ cannot be properly measured (radioactive, very low abundance and right next to the overwhelmingly intense $^{40}\text{Ca}^+$ signal), but the effects are probably not at the detectable level. This is because the initial K of the CAI was almost lost during evaporation, and a good portion of K measured in this sample could have come from surface contamination introduced during sample preparation. Sputter cleaning prior to a spot analysis has removed a lot of surface K, but a small portion of this contaminant may have remained in the sample through “knock-on” effects (e.g., Shimizu and Hart, 1982). This argument has

been used for the Mg isotopic compositions in HAL (Hibonite Allende) type inclusions and laboratory distillation residues (Ireland et al., 1992). In these samples, Mg was strongly depleted (only ppm of Mg left) compared to Ca or Ti, but did not show resolvable mass-dependent fractionations within analytical errors (Fahey et al., 1987; Ireland et al., 1992). We argue that this is also the case for K in CAIs, and thus the intrinsic mass fractionation has no significant impact on the $^{41}\text{K}^*$.

4.2. The initial abundance and distribution of ^{41}Ca inferred from the relationship with ^{26}Al

An understanding of how ^{41}Ca correlates with ^{26}Al in CAIs is crucial for constraining the initial abundance and distribution of ^{41}Ca . ^{26}Al is believed to have been homogeneously distributed at $^{26}\text{Al}/^{27}\text{Al} = 5.2 \times 10^{-5}$ in the (inner) solar nebula during the epoch of CAI formation (at least for large CAIs in CV3 chondrites) (Jacobsen, 2008; Villeneuve et al., 2009). The concordant decay behavior between the two radionuclides found in three Type B CAIs (EGG3, E44 and E65) is used to argue for a cogenetic origin of ^{41}Ca and ^{26}Al , and uniform $^{41}\text{Ca}/^{40}\text{Ca} = 4 \times 10^{-9}$ in the solar nebula (Liu et al., 2012a). However, the inferred ^{26}Al and ^{41}Ca abundances in the three Type A inclusions (two studied here and Allende 7R-19-1 studied by Ito et al. (2006)) are not consistent with the result of synchronicity. If the two short-lived radionuclides had co-decayed in the solar nebula, NWA 3118 #1Nb should have the lowest $^{41}\text{Ca}/^{40}\text{Ca}$ ratio compared to the other two samples because of its sub-canonical $^{26}\text{Al}/^{27}\text{Al}$. However, the opposite is observed in this study.

One possible explanation for the decoupled ^{26}Al and ^{41}Ca abundances would be that the K isotopic compositions of Allende 7R-19-1 and Vigarano 3138 F8 are more disturbed than that of NWA 3118 #1Nb. Isotopic resetting has been frequently invoked to account for sub-canonical $^{26}\text{Al}/^{27}\text{Al}$ ratios seen in many CAIs (e.g., MacPherson et al., 2012). However, the slower diffusivity of K relative to that of Mg (Ito et al., 2006) would imply that the extent to which the K isotopes are disturbed should be slightly less than the Mg isotopes, if mobility is due to thermal effects. Given the fact that the K isotope analyses of Vigarano 3138 F8 and Allende 7R-19-1 were primarily conducted on melilite, and that the Mg isotopic compositions of the CAI minerals (including melilite) appear to be “primitive”, the lack of $^{41}\text{K}^*$ cannot have resulted from isotopic disturbance caused by reheating. Aqueous activities on meteorite parent bodies could potentially compromise an isotopic system (e.g., Lin et al., 2005). While it is true that some Vigarano CAIs have mineralogical records (e.g., veins of calcite and sodalite; MacPherson and Davis, 1993) indicative of aqueous alteration, the Vigarano CAI studied here is free of any secondary mineralization. The Allende 7R-19-1 CAI, on the other hand, contains secondary phases such as grossular along some cracks near the rim of the inclusion, but the area where (Ito et al. (2006)) analyzed is at the center and appears to lack petrographically observable secondary products (Ito et al., 2004). It is therefore less likely that the K isotopic system in the two samples was

affected by a fluid process. From the above reasoning, I argue that the two CAIs most likely formed without the presence of live ^{41}Ca .

The NWA 3118 #1Nb CAI is argued to have been thermally reprocessed based on the petrological features and subcanonical $^{26}\text{Al}/^{27}\text{Al} = (4.64 \pm 0.09) \times 10^{-5}$ (MacPherson et al., 2013). Such thermal events would have also erased radiogenic K excesses that may have existed in the inclusion. The almost identical diffusivities of K and Mg in fassaite (Ito et al., 2003; Zhang et al., 2008) imply that the Mg and K isotopic compositions would be affected to similar degrees, and that the CAI appeared to have remained isotopically undisturbed with regard to both elements after recrystallization (see Section 4.1 for arguments). Scaling the $^{26}\text{Al}/^{27}\text{Al}$ ratio back to 5.2×10^{-5} yields $^{41}\text{Ca}/^{40}\text{Ca} = 1 \times 10^{-8}$, which would plausibly be the initial ^{41}Ca abundance recorded by this NWA CAI.

From the above reasoning, we argue that isotopic resetting is not the reason for the lack of $^{41}\text{K}^*$ in Vigarano 3138 F8 and Allende 7R-19-1. Instead, ^{41}Ca might not have been spatially uniform in the solar nebula during CAI formation, and ^{26}Al and ^{41}Ca abundances could have only been locally correlated. It can be seen in Table 2 that three populations of “true” initial $^{41}\text{Ca}/^{40}\text{Ca}$ ratios could be derived from scaling $^{26}\text{Al}/^{27}\text{Al}$ of each CAI back to 5.2×10^{-5} , implying that (at least) three ^{41}Ca reservoirs characterized by $^{41}\text{Ca}/^{40}\text{Ca}$ of ~ 0 , 4×10^{-9} , and 1×10^{-8} could have been present in the CAI forming region when ^{26}Al was widespread at the canonical level. There is no single $^{41}\text{Ca}/^{40}\text{Ca}$ ratio that could represent the true Solar System initial, and the synchronicity between ^{26}Al and ^{41}Ca in three Type B CAIs found by Liu et al. (2012a) could just be fortuitous. It should be pointed out that the inference for three ^{41}Ca reservoirs/populations is made based on the 6 CAIs. More reservoirs/populations could have existed, but more data are needed to test this.

The correlated absence of ^{26}Al and ^{41}Ca , which was mainly observed in CM2-chondrite platy hibonite crystals, could also be fortuitous in the context of multiple ^{41}Ca reservoirs with different abundances. Most CM2 platy hibonite crystals are characterized either by small magnitudes ($< 5\%$) of ^{26}Mg excesses or by apparent ^{26}Mg deficits by up to 4% relative to terrestrial, regardless of Al/Mg ratio of the grains (Ireland, 1988; Ireland, 1990; Liu et al., 2009; Liu et al., 2012b). This implies initially ^{26}Al -free, Mg-heterogeneous reservoirs in which platy hibonites formed. The presence of such reservoirs could predate the arrival of ^{26}Al from an exotic source (e.g., Sahijpal and Goswami, 1998; Sahijpal et al., 2000; Liu et al., 2009), or the homogenization of ^{26}Al in the CAI forming regions (e.g., Boss, 2007; Boss, 2011). If the ^{41}Ca abundance remained non-uniform in the solar nebula when $^{26}\text{Al}/^{27}\text{Al} = 5.2 \times 10^{-5}$ became widespread, it might have varied to a larger degree before and during mixing. It is therefore plausible that the aforementioned ^{26}Al -free reservoir was also devoid of ^{41}Ca , and hibonite grains that condensed in these regions would have never formed with live ^{26}Al and ^{41}Ca . It should be pointed out that the formation of refractory inclusions in an isotopically heterogeneous solar

nebula would also allow for the existence of samples depleted in ^{26}Al but enriched in ^{41}Ca . The only experimental support available so far comes from a hibonite-rich CAI “022/1” from the CH chondrite Acfer 182, for which $^{41}\text{Ca}/^{40}\text{Ca} = \sim 2 \times 10^{-8}$ and $^{26}\text{Al}/^{27}\text{Al} < 2 \times 10^{-6}$ have been reported (Weber et al., 1995; Srinivasan et al., 2001). However, this evidence should be considered suggestive but not definitive due to large analytical errors associated with the inferred ^{41}Ca abundance and to the fact that the K isotope measurements were performed on a small-geometry ion microprobe. More measurements for ^{41}Ca in samples free of ^{26}Al will be needed to settle this issue.

4.3. The origins of ^{41}Ca in the early Solar System

It has been long argued for the co-delivery of ^{41}Ca and ^{26}Al into an already-formed solar nebula (“late injection”) based on their correlated presence or absence in some refractory inclusions, such as CM-chondrite spinel-hibonite spherules and platy hibonite crystals (e.g., Sahijpal and Goswami, 1998). Although the timing of injection (i.e., into a disk or into a molecular cloud from which the Solar System formed) still remains a matter of debate, the synchronicity between the two radionuclides found in three Type B inclusions (see Table 2) would further strengthen the common origin hypothesis (Liu et al., 2012a). However, the apparent heterogeneous distribution of ^{41}Ca inferred in this study could not be understood in this context, but instead would call for a different explanation for the origin of this radionuclide.

4.3.1. ^{41}Ca as an irradiation product

Considering that ^{26}Al had most likely come into the Solar System as a stellar product because of its homogeneity, the most straightforward explanation for multiple ^{41}Ca reservoirs/populations would be the local production of ^{41}Ca in the solar nebula by energetic charged particle irradiation. A strong argument for intense irradiation occurring in the earliest stage of the Solar System derives from the high but variable abundances of short-lived ^{10}Be ($t_{1/2} = 1.39$ Myr) in CAIs, with $^{10}\text{Be}/^9\text{Be}$ ranging from 3×10^{-4} to 1×10^{-2} (McKeegan et al., 2000; Sugiura et al., 2001; Marhas et al., 2002; MacPherson et al., 2003; Chaussidon et al., 2006; Liu et al., 2009; Liu et al., 2010; Gounelle et al., 2013; Wielandt et al., 2012; Srinivasan and Chaussidon, 2013). Such a variability can be understood as a consequence of proton fluence fluctuations (McKeegan et al., 2000; Chaussidon et al., 2006; Liu et al., 2010; Gounelle et al., 2013; Srinivasan and Chaussidon, 2013). With a favorable target chemistry, such as a CAI-like composition (i.e., enriched in refractory elements), irradiation by gradual flares (which have larger fractions of higher-energy projectiles; Lee et al., 1998) can also be conducive to producing ^{41}Ca in addition to ^{10}Be , but not ^{26}Al . This would allow for a spectrum of $^{41}\text{Ca}/^{40}\text{Ca}$ ratios characterizing different CAIs, as is the case for ^{10}Be .

One major, well-known problem with any proton irradiation model is the overproduction of ^{41}Ca relative to ^{10}Be . For example, calculations have shown that the proton fluence capable of producing $^{10}\text{Be}/^9\text{Be}$ at 9×10^{-4} in CAIs

would yield $^{41}\text{Ca}/^{40}\text{Ca} \sim (2\text{--}4) \times 10^{-7}$, assuming a short ($\ll t_{1/2}$ of ^{41}Ca) irradiation time (e.g., Lee et al., 1998; Herzog et al., 2011). This problem could be somewhat alleviated if the Solar System formed with a baseline $^{10}\text{Be}/^9\text{Be}$ ratio. Wielandt et al. (2012) proposed that the molecular cloud from which the Solar System formed was characterized by $^{10}\text{Be}/^9\text{Be} = 3 \times 10^{-4}$, as this value was recorded by ^{26}Al -free FUN (Fractionated and Unknown Nuclear anomalies) CAIs Axtell 2771 and KT-1, which were presumably formed before usual CAIs. Based on this inference, Tatischeff et al. (2014) proposed that this background ^{10}Be abundance would be possible if one takes into account the total ^{10}Be production from two sources: irradiation of the presolar molecular cloud by background Galactic Cosmic Rays, and by cosmic rays produced by ≥ 50 supernovae exploding in a superbubble of hot gas generated by a large cluster of at least 20,000 stars. The alternative, which is favored by Tatischeff et al. (2014), to the latter mechanism is irradiation of the cloud by accelerated cosmic rays escaped from an isolated supernova remnant. Any $^{10}\text{Be}/^9\text{Be}$ ratio higher than 3×10^{-4} seen in CAIs could be a result of in situ production of ^{10}Be by solar energetic particle spallation. In this context, the needed dosage of protons to match the observed $^{10}\text{Be}/^9\text{Be}$ ratios would be lessened, and so would be the collaterally produced ^{41}Ca abundances. A simple back-of-the-envelope calculation shows that if the Solar System did begin with homogeneous $^{10}\text{Be}/^9\text{Be} = 3 \times 10^{-4}$, the required proton fluence would drop by 33% and 50%, respectively, for a CAI having an initial $^{10}\text{Be}/^9\text{Be}$ ratio of 9×10^{-4} and 6×10^{-4} . As a result, the amounts of irradiation-produced ^{41}Ca would be reduced by the same percentages to the level approximately of 10^{-7} , which is still too high by an order of magnitude.

In the context of Solar System inheriting homogeneous $^{10}\text{Be}/^9\text{Be} = 3 \times 10^{-4}$ from the parental molecular cloud, the predicted spallogenic $^{41}\text{Ca}/^{40}\text{Ca}$ ratios remain high compared to the inferred ones in CAIs. However, it is possible that the $^{10}\text{Be}/^9\text{Be}$ ratio that characterized the molecular cloud could have been not as homogeneous as was assumed in the model of Tatischeff et al. (2014). If the lack of ^{26}Al and preservation of large nuclear anomalies in FUN CAIs are indicative of antiquity, CM-chondrite platy hibonite crystals (see above) should have been as old as (if not older than) FUN inclusions because they carry isotope anomalies in neutron-rich ^{48}Ca and ^{50}Ti up to $\sim 40\%$ (cf. $< 2\%$ in FUN inclusions) (e.g., Lee et al., 1979; Zinner et al., 1986; Fahey et al., 1987; Ireland, 1990; Sahijpal et al., 2000; Liu et al., 2009). These platy hibonite grains have a well-defined $^{10}\text{Be}/^9\text{Be}$ ratio of $(5.3 \pm 1.0) \times 10^{-4}$ (Liu et al., 2009; Liu et al., 2010). Therefore, the parental molecular cloud's $^{10}\text{Be}/^9\text{Be}$ could have spatially varied between 3×10^{-4} and 5×10^{-4} . A variation at this level is not implausible considering the assumptions used in the calculations. To arrive at $^{10}\text{Be}/^9\text{Be} = 3 \times 10^{-4}$ in the Solar System's parental cloud, Tatischeff et al. (2014) have to assume in their favored model that the supernova remnant must have expanded in a medium with the hydrogen number density of 1 cm^{-3} before cosmic rays that escaped from this remnant irradiated the cloud. If a molecular cloud was

directly hit by cosmic rays inside the supernova remnant, the resulting $^{10}\text{Be}/^9\text{Be}$ ratio would be approximately one order of magnitude higher than 3×10^{-4} . It is known that a molecular cloud can be clumpy, with a large variation in density (e.g., Norman and Silk, 1980), and the ^{10}Be production is proportional to the hydrogen number density of the molecular cloud (Tatischeff et al., 2014). It is therefore conceivable that the Solar System could have formed with somewhat heterogeneous $^{10}\text{Be}/^9\text{Be}$ as a background. If so, the fluence needed for a CAI, which had incorporated $^{10}\text{Be}/^9\text{Be}$ as high as 5×10^{-4} when it formed, to acquire the final $^{10}\text{Be}/^9\text{Be}$ ratio of 9×10^{-4} would yield $^{41}\text{Ca}/^{40}\text{Ca} \sim 6 \times 10^{-8}$. Since most CV3 CAIs are characterized by $^{10}\text{Be}/^9\text{Be}$ between $(4\text{--}7) \times 10^{-4}$, the expected $^{41}\text{Ca}/^{40}\text{Ca}$ in them would be consistent within model uncertainties with the $^{41}\text{Ca}/^{40}\text{Ca}$ range ($\sim 0\text{--}1 \times 10^{-8}$) proposed in this paper. However, this model cannot satisfactorily provide an explanation for the $^{41}\text{Ca}\text{--}^{10}\text{Be}$ characteristics in the E44 and E65 CAIs. The two inclusions have $^{10}\text{Be}/^9\text{Be} = (7\text{--}8) \times 10^{-4}$ (McKeegan et al., 2001; Srinivasan and Chaussidon, 2013), but their inferred “initial” $^{41}\text{Ca}/^{40}\text{Ca}$ ratios are only $\sim 4 \times 10^{-9}$ (Liu et al., 2012a), a factor of $\sim 7\text{--}10$ lower than the expected level from this model. More coordinated $^{10}\text{Be}\text{--}^{41}\text{Ca}$ analyses of CAIs are needed to understand whether these two CAIs are just outliers and to test the validity of this model.

4.3.2. ^{41}Ca as a stellar product

An alternative explanation to irradiation for the seemingly heterogeneous distribution of ^{41}Ca in the early Solar System involves that each CAI represents a mixture of old, radioactivity-free pre-existing material (e.g., interstellar grains) and freshly synthesized short-lived radioactivities carried by different carrier grains from nearby evolved stars. This scenario is possible if the Solar System formed in a cloud enriched in live ^{26}Al and ^{41}Ca , which were delivered by stellar winds either from a single Wolf–Rayet (W–R) star (e.g., Tatischeff et al., 2010; Gounelle and Meynet, 2012; Gounelle, 2015) or from multiple W–R stars (e.g., Gaidos et al., 2009; Young, 2014). Different models invoke different astrophysical assumptions; discerning which model could better account for the observed ^{26}Al homogeneity and ^{41}Ca heterogeneity is beyond the scope of this paper. The following discussion is solely based on the nature of nucleosynthesis and mixing processes.

If winds from W–R stars contaminated the Sun’s natal molecular cloud, the arrival of ^{26}Al and ^{41}Ca in the cloud could be temporally decoupled due to the nucleosynthetic processes (see Arnould et al., 1997; Arnould et al., 2006 for details). ^{26}Al is produced by core H-burning and is carried away by winds during the WN (N-rich) phase. This stage lasts for some 10^5 years before a W–R star enters the He-burning WC–WO (C–O rich) phase, during which ^{41}Ca , an *s*-process isotope, is synthesized and released from the star(s). This allows that ^{26}Al be collected by the Sun’s natal molecular cloud and mixed with pre-existing molecular cloud material for $\sim 10^5$ years before ^{41}Ca was present, assuming all massive stars evolved into the W–R phase at

the same time. ^{26}Al and ^{41}Ca would most likely condense into refractory grains in stellar winds due to their refractory and lithophile nature (e.g., Ebel, 2000) and then were delivered into the molecular cloud. The initial distribution of the grains in the molecular cloud could have been extremely heterogeneous, regardless of the models. For example, in the model of Gounelle and Meynet (2012), only one side of the dense collected shell in which the Solar System formed would have been enriched in ^{26}Al , and a timescale of at least some 10^5 years would be needed to homogenize the ^{26}Al distribution across the shell. Similarly, Gaidos et al. (2009) acknowledged that the grains that carried radioactivities would be stopped at the surface of a molecular cloud because of the increased surface gas densities caused by the expanding W–R winds. The timescales needed to transport the carrier grains into the cloud cannot be well constrained owing to poor understandings of the kinematics, but can be approximated by using the turbulent mixing timescale in an un-shocked molecular cloud, which is $\sim 2 \times 10^5$ years across 0.1 parsec (pc) (Pan et al., 2012), roughly the size of a dense molecular cloud core which formed the Solar System (Jijina et al., 1999). Given the typical size of a molecular cloud (10–100 pc), approximately $10^7\text{--}10^8$ years would be needed to completely homogenize the grain distribution within it. This timescale is longer than the lifetime of a cloud ($\leq 10^7$ years; Larson, 1981), and the radionuclides would have completely decayed away. Therefore, Solar System formation must have taken place when ^{26}Al carrier grains were heterogeneously distributed in the cloud, and the abundance and distribution of ^{26}Al that the Solar System formed with depend on the location and time. The same is true for ^{41}Ca , except that its carrier grains would have experienced less mixing compared to those of ^{26}Al , and thus populated more non-uniformly within the cloud. In addition, because of the shorter half-life, the abundance dispersion for ^{41}Ca is expected to be larger than that for ^{26}Al based on the following relationship: $\sigma_x \propto (\frac{\tau_{\text{mixing}}}{\tau_x})$ (Jobson et al., 1999), where x is the radioisotope of interest, τ_{mixing} is the mixing timescale, and τ_x is the mean-life of the radionuclide. The forming Solar System incorporated ^{26}Al and ^{41}Ca carrier grains, the former of which may have been more widely and evenly spread than the latter because of additional mixing, along with radioactivity-free interstellar dust. These radioactivity carriers had to be thermally processed, evaporated, and then re-condensed into the refractory inclusions. The first solids that formed before homogenization would be expected to have recorded variations in ^{26}Al and ^{41}Ca , and the smaller the inclusion size, the larger the variation due to the relative proportions of old and new material sampled from the nebula gas.

This scenario can qualitatively explain the observed isotopic signatures in meteoritic refractory inclusions. CM platy hibonite crystals most likely formed in the region(s) free of ^{26}Al but instead characterized by large Mg (and neutron-rich isotopes) isotopic heterogeneities, perhaps carried by old interstellar dust (see Liu et al., 2012b). As stated above, the lack of ^{26}Al does not necessarily guarantee the absence of ^{41}Ca in these regions because the carriers of ^{26}Al and ^{41}Ca might not have been spatially correlated.

Some evidence for such reservoirs is provided by the hibonite-rich CAI “022/1” from the CH chondrite Acfer 182 (see above, Weber et al., 1995; Srinivasan et al., 2001). The ^{26}Al variability, which ranges from $^{26}\text{Al}/^{27}\text{Al} = 6 \times 10^{-6}$ to 6×10^{-5} , found in CM-chondrite spinel-hibonite spherules by Liu et al. (2012b) could be derived from the formation of these inclusions during the homogenization of ^{26}Al . The $^{41}\text{Ca}/^{40}\text{Ca}$ ratios in the spinel-hibonite spherules should also have scatter, but to a larger magnitude. However, this is still poorly constrained because of the analytical challenges (small ($\leq 50 \mu\text{m}$) samples, pervasive K contamination, etc.). Most CAIs formed after ^{26}Al had arrived at homogeneity with $^{26}\text{Al}/^{27}\text{Al} = 5.2 \times 10^{-5}$ in the solar nebula. ^{41}Ca at that time could have still been heterogeneous, but to a much lesser extent, because its carriers were more sparse than those of ^{26}Al at the beginning of the Solar System.

The scenario described above does not take into account that the W–R winds could be clumpy (e.g., Lépine and Moffat, 2008), and that the formation history of massive stars is not monotonic (e.g., Hartmann, 2001). The more realistic situation is certainly more complicated, but would not change the fact that the delivery of ^{26}Al into the molecular cloud preceded that of ^{41}Ca , and the former should always be more thoroughly mixed than the latter when the Solar System formed.

5. CONCLUSION

Analysis of two Type A CAIs, NWA 3118 #1Nb (CTA) and Vigarano 3138 F8 (FTA), from reduced CV3 chondrites, yields $^{41}\text{Ca}/^{40}\text{Ca} = (4.6 \pm 1.9) \times 10^{-9}$ and $(-2.0 \pm 2.5) \times 10^{-9}$, respectively. Their ^{41}Ca abundances do not correlate with the $^{26}\text{Al}/^{27}\text{Al}$ ratios, inconsistent with the expectation from the concordant decay behavior between ^{26}Al and ^{41}Ca proposed by Liu et al. (2012a). Based on the available dataset, it appears that there were at least three reservoirs/populations of $^{41}\text{Ca}/^{40}\text{Ca}$ (~ 0 , 4×10^{-9} and 1×10^{-8}) in the solar nebula when $^{26}\text{Al}/^{27}\text{Al}$ was widespread at 5.2×10^{-5} . The apparent heterogeneity of ^{41}Ca can be understood in the context of early Solar System irradiation, but it requires the presence of “preexisting” ^{10}Be , whose abundance was heterogeneous at the level of $^{10}\text{Be}/^9\text{Be} = (3\text{--}5) \times 10^{-4}$, in the Solar System’s parental cloud. This background ^{10}Be could have originated from the irradiation of Sun’s parental molecular cloud by cosmic rays accelerated by an isolated supernova remnant. However, this model cannot satisfactorily explain the ^{41}Ca abundances inferred for the Efremovka E44 and E65 CAIs by Liu et al. (2012a). It is also plausible that the Solar System derived both ^{41}Ca and ^{26}Al from the parental molecular cloud contaminated by winds of Wolf–Rayet stars. Because of the difference in the arrival time, ^{26}Al carrier grains could have experienced a larger degree of mixing in the molecular cloud than those of ^{41}Ca so that the latter would have been more sparse and were not necessarily spatially correlated with the former in the forming Solar System. This could qualitatively explain why ^{26}Al and ^{41}Ca seemed to have different distributions when CV3

CAIs formed. It is important to note that the above scenarios are constructed based on ^{26}Al and ^{41}Ca data reported for only 6 CAIs, and are subject to change should more high quality data become available.

ACKNOWLEDGEMENTS

This work is dedicated to Dr. Ian Hutcheon, who pioneered the isotopic analysis of ^{41}Ca – ^{41}K system in meteoritic refractory inclusions. The author would like to thank Marc Chaussidon, Kevin McKeegan and Ed Young (in alphabetical order) for insightful discussions and comments on the draft of this paper. Critical reviews by Dr. Andy Davis of the University of Chicago and an anonymous reviewer greatly improved the quality of this paper. Dr. Qing-zhu Yin is thanked for his editorial efforts. The samples used in this study were kindly provided by Dr. Glenn MacPherson of the Smithsonian Institution. The UCLA ion microprobe facility is partially supported by a grant from the NSF Instrumentation and Facilities program, for which the author is grateful.

REFERENCES

- Arnould M., Paulus G. and Meynet G. (1997) Short-lived radionuclide production by non-exploding Wolf–Rayet stars. *Astro. Astrophys.* **321**, 452–464.
- Arnould M., Goriely S. and Meynet G. (2006) The production of short-lived radionuclides by new non-rotating and rotating Wolf–Rayet model stars. *Astro. Astrophys.* **453**, 653–659.
- Boss A. P. (2007) Evolution of the solar nebula. VIII. Spatial and temporal heterogeneity of short-lived radioisotopes and stable oxygen isotopes. *Astrophys. J.* **660**, 1707–1714.
- Boss A. P. (2011) Evolution of the solar nebula. IX. Gradients in the spatial heterogeneity of the short-lived radioisotopes ^{60}Fe and ^{26}Al and the stable oxygen isotopes. *Astrophys. J.* **739**, 61–71.
- Chaussidon M., Robert F. and McKeegan K. D. (2006) Li and B isotopic variations in an Allende CAI: evidence for the in situ decay of short-lived ^{10}Be and for the possible presence of the short-lived nuclide ^7Be in the early solar system. *Geochim. Cosmochim. Acta* **70**, 224–245.
- Coath C. D., Steele R. C. J. and Lunn W. F. (2013) Statistical bias in isotope ratios. *J. Anal. At. Spectrom.* **28**, 52–58.
- Ebel D. S. (2000) Variations on solar condensation: sources of interstellar dust nuclei. *J. Geophys. Res.* **105**, 10363–10370.
- Fahey A. J., Goswami J. N., McKeegan K. D. and Zinner E. K. (1987) ^{26}Al , ^{244}Pu , ^{50}Ti , REE, and trace element abundances in hibonite grains from CM and CV meteorites. *Geochim. Cosmochim. Acta* **51**, 329–350.
- Gaidos E., Krot A. N., Williams J. P. and Raymond S. N. (2009) ^{26}Al and the formation of the solar system from a molecular cloud contaminated by Wolf–Rayet winds. *Astrophys. J.* **696**, 1854–1863.
- Garner E. L., Murphy T. J., Gramlich J. W., Paulsen P. J. and Barnes I. L. (1975) Absolute isotopic abundance ratio and the atomic weight of a reference sample of potassium. *J. Res. Nat. Bur. Stan.* **79A**, 713–725.
- Gounelle M. (2015) The abundance of ^{26}Al -rich planetary systems in the Galaxy. *Astro. Astrophys.* **582** A26.
- Gounelle M. and Meynet G. (2012) Solar system genealogy revealed by extinct short-lived radionuclides in meteorites. *Astro. Astrophys.* **545**, A4.
- Gounelle M., Shu F. H., Shang H., Glassgold A. E., Rehm K. E. and Lee T. (2006) The irradiation origin of beryllium radioisotopes and other short-lived radionuclides. *Astrophys. J.* **640**, 1163–1170.

- Gounelle M., Chaussidon M. and Rollion-Bard C. (2013) Variable and extreme irradiation conditions in the early solar system inferred from the initial abundance of ^{10}Be in Isheyevo CAIs. *Astrophys. J. Lett.* **763**, L33.
- Hartmann L. (2001) On age spreads in star-forming regions. *Astronom. J.* **121**, 1030–1039.
- Herzog G. F., Caffee M. W., Faestermann T., Hertenberger R., Korschinek G., Leya I., Reedy R. C. and Sistierson J. M. (2011) Cross sections from 5 to 35 MeV for the reactions $^{nat}\text{Mg}(^3\text{He}, x)^{26}\text{Al}$, $^{27}\text{Al}(^3\text{He}, x)^{26}\text{Al}$, $^{nat}\text{Ca}(^3\text{He}, x)^{41}\text{Ca}$, and $^{nat}\text{Ca}(^3\text{He}, x)^{36}\text{Cl}$: implications for early irradiation in the solar system. *Meteor. Planet. Sci.* **46**, 1427–1446.
- Huss G. R., Meyer B. S., Srinivasan G., Goswami J. N. and Sahijpal S. (2009) Stellar sources of the short-lived radionuclides in the early solar system. *Geochim. Cosmochim. Acta* **73**, 4922–4945.
- Hutcheon I. D., Armstrong J. T. and Wasserburg G. J. (1984) Excess ^{41}K in allende CAI: confirmation of a Hint. *Lunar Planet. Sci.* **XV**, 387–388 (abstr.).
- Ireland T. R. (1988) Correlated morphological, chemical, and isotopic characteristics of hibonites from the Murchison carbonaceous chondrite. *Geochim. Cosmochim. Acta* **52**, 2827–2839.
- Ireland T. R. (1990) Presolar isotopic and chemical signatures in hibonite-bearing refractory inclusions from the Murchison carbonaceous chondrite. *Geochim. Cosmochim. Acta* **54**, 3219–3237.
- Ireland T. R., Zinner E. K., Fahey A. J. and Esat T. M. (1992) Evidence for distillation in the formation of HAL and related hibonite inclusions. *Geochim. Cosmochim. Acta* **56**, 2503–2520.
- Ito M., Ganguly J. (2003) Diffusion Kinetics of K in Melilite and Diopside: Constraints on the Accretion Time Scale and Thermal History of CAI Parent Body, *66th Meteoritic Society Meeting #5134* (abstr.).
- Ito M., Nagasawa H. and Yurimoto H. (2004) Oxygen isotopic SIMS analysis in Allende CAI: details of the very early thermal history of the solar system. *Geochim. Cosmochim. Acta* **68**(13), 2905–2923.
- Ito M., Nagasawa H. and Yurimoto H. (2006) A study of Mg and K isotopes in Allende CAIs: implications to the time scale for the multiple heating processes. *Meteor. Planet. Sci.* **41**, 1871–1881.
- Jacobsen B., Zhu Yin Q., Moynier F., Amelin Y., Krot A. N., Nagashima K., Hutcheon I. D. and Palme H. (2008) ^{26}Al - ^{26}Mg and ^{207}Pb - ^{206}Pb systematics of Allende CAIs: canonical solar initial $^{26}\text{Al}/^{27}\text{Al}$ ratio reinstated. *Earth Planet. Sci. Lett.* **272**, 353–364.
- Jijina J., Myers P. C. and Adams F. C. (1999) Dense cores mapped in ammonia: a database. *Astrophys. J. Suppl.* **125**, 161–236.
- Jobson B. T., McKeen S. A., Parrish D. D., Fehsenfeld F. C., Blake D. R., Goldstein A. H., Schauffler S. M. and Elkins J. W. (1999) Trace gas mixing ratio variability versus lifetime in the troposphere and stratosphere: observations. *J. Geophys. Res. Atmos.* **104**(D13), 16091–16113.
- Larson R. B. (1981). *Turbulence and star formation in molecular clouds* **194**, 809–826.
- Lee T., Russell W. A. and Wasserburg G. J. (1979) Calcium isotopic anomalies and the lack of aluminum-26 in an unusual Allende inclusion. *Astrophys. J.* **228**, L93–L98.
- Lee T., Shu F. H., Shang H., Glassgold A. E. and Rehm K. E. (1998) Protostellar cosmic rays and extinct radioactivities in meteorites. *Astrophys. J.* **506**, 898–912.
- Lépine S. and Moffat A. F. J. (2008) Direct spectroscopic observations of clumping in O-star winds. *Astronom. J.* **136** (2), 548.
- Lin Y., Guan Y., Leshin L. A., Ouyang Z. and Wang D. (2005) Short-lived chlorine-36 in a Ca- and Al-rich inclusion from the Ningqiang carbonaceous chondrite. *Proc. Natl. Acad. Sci. U. S. A.* **102**(5), 1306–1311.
- Liu M.-C., McKeegan K. D., Goswami J. N., Marhas K. K., Sahijpal S., Ireland T. R. and Davis A. M. (2009) Isotopic records in CM hibonites: implications for timescales of mixing of isotope reservoirs in the solar nebula. *Geochim. Cosmochim. Acta* **73**, 5051–5079.
- Liu M.-C., Nittler L. R., Alexander C. M. O. and Lee T. (2010) Lithium-beryllium-boron isotopic compositions in meteoritic hibonite: implications for origin of ^{10}Be and early solar system irradiation. *Astrophys. J.* **719**, L99–L103.
- Liu M.-C., Chaussidon M., Srinivasan G. and McKeegan K. D. (2012a) A lower initial abundance of short-lived ^{41}Ca in the early solar system and its implications for solar system formation. *Astrophys. J.* **761**, 137.
- Liu M.-C., Chaussidon M., Göpel C. and Lee T. (2012b) A heterogeneous solar nebula as sampled by CM hibonite grains. *Earth Planet. Sci. Lett.* **327**, 75–83.
- MacPherson G. J. and Davis A. M. (1993) A petrologic and ion microprobe study of a Vigarano Type B refractory inclusion – evolution by multiple stages of alteration and melting. *Geochim. Cosmochim. Acta* **57**, 231–243.
- MacPherson G. J., Huss G. R. and Davis A. M. (2003) Extinct ^{10}Be in Type A calcium–aluminum-rich inclusions from CV chondrites. *Geochim. Cosmochim. Acta* **67**, 3165–3179.
- MacPherson G. J., Kita N. T., Ushikubo T., Bullock E. S. and Davis A. M. (2012) Well-resolved variations in the formation ages for Ca–Al-rich inclusions in the early Solar System. *Earth Planet. Sci. Lett.* **331**, 43–54.
- MacPherson G. J., Ushikubo T., Kita N. T., Ivanova M. A., Bullock E. S. and Davis A. M. (2013) Petrologic and $^{26}\text{Al}/^{27}\text{Al}$ isotopic studies of type A CAIs and documentation of the fluffy type A – compact Type A – Type B CAI evolutionary transition. *Lunar Planet. Sci.*, #1530 (abstr.).
- Marhas K. K., Goswami J. N. and Davis A. M. (2002) Short-lived nuclides in hibonite grains from murchison: evidence for solar system evolution. *Science* **298**, 2182–2185.
- McKeegan K. D., Chaussidon M. and Robert F. (2000) Incorporation of short-lived ^{10}Be in a calcium–aluminum-rich inclusion from the Allende meteorite. *Science* **289**, 1334–1337.
- McKeegan K. D., Chaussidon M., Krot A. N., Robert F., Goswami J. N. and Hutcheon I. D. (2001) Extinct radionuclide abundances in Ca, Al-rich Inclusions from the CV chondrites allende and efremovka: a search for synchronicity. *Lunar Planet. Sci.*, #2175 (abstr.).
- Niederer F. R. and Papanastassiou D. A. (1984) Ca isotopes in refractory inclusions. *Geochim. Cosmochim. Acta* **48**, 1279–1293.
- Norman C. and Silk J. (1980) Clumpy molecular clouds – a dynamic model self-consistently regulated by T Tauri star formation. *Astrophys. J.* **238**, 158–174.
- Ogliore R. C., Huss G. R. and Nagashima K. (2011) Ratio estimation in SIMS analysis. *Nucl. Instrum. Methods Phys. Res. B* **269**, 1910–1918.
- Pan L., Desch S. J., Scannapieco E. and Timmes F. X. (2012) Mixing of clumpy supernova ejecta into molecular clouds. *Astrophys. J.* **756**(1), 102.
- Richter F. M., Janney P. E., Mendybaev R. A., Davis A. M. and Wadhwa M. (2007) Elemental and isotopic fractionation of Type B CAI-like liquids by evaporation. *Geochim. Cosmochim. Acta* **71**, 5544–5564.
- Richter F. M., Mendybaev R. A., Christensen J. N., Ebel D. and Gaffney A. (2011) Laboratory experiments bearing on the

- origin and evolution of olivine-rich chondrules. *Meteorit. Planet. Sci.* **46**, 1152–1178.
- Sahijpal S. and Goswami J. N. (1998) Refractory phases in primitive meteorites devoid of ^{26}Al and ^{41}Ca : representative samples of first solar system solids? *Astrophys. J.* **509**, L137–L140.
- Sahijpal S., Goswami J. N. and Davis A. M. (2000) K, Mg, Ti and Ca isotopic compositions and refractory trace element abundances in hibonites from CM and CV meteorites: implications for early solar system processes. *Geochim. Cosmochim. Acta* **64**, 1989–2005.
- Shimizu N. and Hart S. R. (1982) Applications of the ion microprobe to geochemistry and cosmochemistry. *Ann. Rev. Earth Planet. Sci.* **10**, 483.
- Srinivasan G. and Chaussidon M. (2013) Constraints on ^{10}Be and ^{41}Ca distribution in the early solar system from ^{26}Al and ^{10}Be studies of Efremovka CAIs. *Earth Planet. Sci. Lett.* **374**, 11–23.
- Srinivasan G., Sahijpal S., Ulyanov A. A. and Goswami J. N. (1996) Ion microprobe studies of Efremovka CAIs: II. Potassium isotope composition and ^{41}Ca in the early Solar System. *Geochim. Cosmochim. Acta* **60**, 1823–1835.
- Srinivasan G., Bischoff A (2001) Ca–K and Al–Mg studies of CAIs from CH and CR chondrites, *64th Meteoritic Society Meeting* 36, A196 (abstr.).
- Sugiura N., Shuzou Y. and Ulyanov A. (2001) Beryllium-boron and aluminum-magnesium chronology of calcium-aluminum-rich inclusions in CV chondrites. *Meteor. Planet. Sci.* **36**, 1397–1408.
- Sylvester P. J., Simon S. B. and Grossman L. (1993) Refractory inclusions from the Leoville, Efremovka, and Vigarano C3V chondrites – major element differences between Types A and B, and extraordinary refractory siderophile element compositions. *Geochim. Cosmochim. Acta* **57**, 3763–3784.
- Tatischeff V., Duprat J. and de Séréville N. (2010) A runaway Wolf–Rayet star as the origin of ^{26}Al in the early Solar System. *Astrophys. J.* **714**, L26–L30.
- Tatischeff V., Duprat J. and de Séréville N. (2014) Light-element Nucleosynthesis in a molecular cloud interacting with a supernova remnant and the origin of beryllium-10 in the protosolar nebula. *Astrophys. J.* **796**(2), 124.
- Villeneuve J., Chaussidon M. and Libourel G. (2009) Homogeneous distribution of ^{26}Al in the Solar System from the Mg isotopic composition of chondrules. *Science* **325**, 985–988.
- Wasserburg G. J., Busso M., Gallino R. and Nollett K. M. (2006) Short-lived nuclei in the early solar system: possible AGB sources. *Nucl. Phys. A* **777**, 5–69.
- Wasserburg G. J., Wimpenny J. and Yin Q.-Z. (2012) Mg isotopic heterogeneity, Al–Mg isochrons, and canonical $^{26}\text{Al}/^{27}\text{Al}$ in the early solar system. *Meteor. Planet. Sci.* **47**, 1980–1997.
- Weber D., Zinner E. and Bischoff A. (1995) Trace element abundances and magnesium, calcium, and titanium isotopic compositions of grossite-containing inclusions from the carbonaceous chondrite Acfer 182. *Geochim. Cosmochim. Acta* **59** (4), 803–823.
- Wielandt D., Nagashima K., Krot A. N., Huss G. R., Ivanova M. A. and Bizzarro M. (2012) Evidence for multiple sources of ^{10}Be in the early solar system. *Astrophys. J. Lett.* **748**, L25.
- Young E. D. (2014) Inheritance of solar short- and long-lived radionuclides from molecular clouds and the unexceptional nature of the solar system. *Earth Planet. Sci. Lett.* **392**, 16–27.
- Young E. D., Simon J. I., Galy A., Russell S. S., Tonui E. and Lovera O. (2005) Supra-canonical $^{26}\text{Al}/^{27}\text{Al}$ and the residence time of CAIs in the solar protoplanetary disk. *Science* **308**, 223–227.
- Zhang X.-Y., Ganguly J. and Ito M. (2008) Self diffusivities of Ca and Mg in clinopyroxene: experimental studies and planetary applications. *Lunar Planet. Sci.*, #2049 (abstr.).
- Zinner E. K., Fahey A. J., Goswami J. N., Ireland T. R. and McKeegan K. D. (1986) Large ^{48}Ca anomalies are associated with ^{50}Ti anomalies in Murchison and Murray hibonites. *Astrophys. J.* **311**, L103–L107.

Associate editor: Qing-Zhu Yin